Received: 29 June 2025 | Revised: 15 November 2025 | Accepted: 27 December 2025

DOI: 10.1002/qj.70123

Quarterly Journal of the Royal Meteorological Society RMetS

RESEARCH ARTICLE

Covariance of the intertropical discontinuity and African easterly jet in Sahelian wet and dry years

Marian Amoakowaah Osei[1,2] | **Cornelia Klein**[2] | **Christopher M. Taylor**[2,3] | **Douglas J. Parker**[4,5,6] | **Michael Baidu**[4]

[1]Met Office, FitzRoy Road, Exeter, UK

[2]Water and Climate Science, UK Centre for Ecology and Hydrology, Crowmarsh Gifford, UK

[3]National Centre for Earth Observation, Wallingford, UK

[4]School of Earth and Environment, University of Leeds, Leeds, UK

[5]NCAS, University of Leeds, Leeds, UK

[6]NORCE Norwegian Research Centre AS, Bergen, Norway

Correspondence
Marian Amoakowaah Osei, Met Office, FitzRoy Road, Exeter, Devon, EX1 3PB, UK.
Email: marian.osei@metoffice.gov.uk

Funding information
Natural Environment Research Council, Grant/Award Number: NE/X017419/1; Royal Society, Grant/Award Number: NIF\R1\211183

Abstract

This study examines the covariance between the intertropical discontinuity (ITD) and African easterly jet (AEJ) over the West African Sahel in wet and dry year composites, using a decade of reanalysis data. ITD and AEJ positions are strongly correlated, with a more pronounced linear relationship across wet years due to the sensitivity to an intensified monsoonal flow. Whereas the AEJ's diurnal cycle shows little meridional displacement, its intensity and the ITD position show clear diurnal cycles. Considering land-surface controls, we find surface heat flux anomalies around 15°N to modify low-level temperature and sensible heat flux gradients, affecting the thermal wind and shifting the AEJ core to 1° south of gradient maxima. More northward gradients, and hence a more northerly AEJ, occur in wet years, with a smaller shift in the ITD. Consequently, the ITD–AEJ distance narrows in wet years, driven by enhanced convective activity. Correspondingly, we find that peak frequencies of colder, more intense convective systems shift further north in wet years, whereas the southern location of warmer systems remains similar between composites. This is due to deep moist conditions prevailing south of the AEJ for both composites, favouring warm mesoscale convective system formation in a weakly sheared environment. In contrast, convective available potential energy and shear maxima shift north and align with the AEJ in wet years, displacing the environment for colder storm development. The ITD shows less sensitivity to anomalies in surface processes but may influence isolated storm events close to its positioning. These findings improve understanding of ITD–AEJ interactions and their sensitivity to soil moisture conditions, highlighting the need for high-resolution modelling to capture local feedback mechanisms.

KEYWORDS

African easterly jet, intertropical discontinuity, mesoscale convective systems, soil moisture, surface heat flux

1 | INTRODUCTION

The seasonal north–south oscillation of the intertropical discontinuity (ITD) and African easterly jet (AEJ) is an important feature of the West African monsoon system, affecting the initiation and maintenance of Sahelian rainfall. Each of these features is known to control the rainfall, and each is known to be closely tied to the regional temperature and moisture gradients. But there has been no systematic study of the way in which the ITD and AEJ may covary, and may jointly or independently influence the precipitation. The ITD is the zone of low-level convergence of cool, moist monsoonal southwesterly air and the hot dry Saharan air over continental West Africa (Cornforth *et al.*, 2017). It marks a critical baroclinic region that maps the northward extent of the moist monsoon air that favours moist convection and rainfall activities (Cornforth *et al.*, 2017; Nicholson, 2018). Owing to the sloping baroclinic zone, the ITD is displaced northward of the main precipitation zone of the monsoon, and this makes it different from the global oceanic feature, the intertropical convergence zone, a low-level convergence of southeasterly and northeasterly trade winds around the Equator, co-located with the maximum rainfall zone over the ocean—see extensive explanations in Parker and Diop-Kane (2017) and Nicholson (2018).

The AEJ results from the temperature contrast between the hot Saharan air mass and the cooler, more humid air over the Guinea Coast (Cook, 1999; Parker *et al.*, 2005; Sultan *et al.*, 2007). The AEJ system is known to be in approximate thermal wind balance, hence the strength of the baroclinic zone to the south of the ITD dictates positioning and speed of the AEJ, which in turn interacts with the organisation of deep convection (Parker *et al.*, 2005; Tompkins *et al.*, 2005). Dry convection at the latitude of the ITD is associated with cyclonic circulation over surface troughs, which influences the monsoon westerlies, and an anticyclonic circulation at around 600 mb overlying the Saharan heat low, which affects the speed of the AEJ (Sultan & Janicot, 2003). Maximum rainfall also occurs approximately 200 km south of the ITD, where moisture content is high and conditions favour strong AEJ-related shear and vorticity (Thorncroft & Blackburn, 1999). However, near the ITD, a dry convective environment usually prevails with strong subsidence that suppresses storm activities (Nicholson, 2009).

The variability in ITD and AEJ is also intricately linked to the partitioning of surface energy into sensible and latent heat fluxes (SH and LH respectively), a process strongly influenced by soil moisture (SM) dynamics. Negative SM and latent heat gradients between the Guinea Coast and Saharan desert induces a positive temperature gradient that drives the AEJ northward (Cook, 1999; Wu *et al.*, 2009). Significantly positive SM anomalies following dry periods in the Sahel can also trigger substantial northward displacements of the ITD, potentially spanning several 100 km (Talib *et al.*, 2022). Mutton *et al.* (2022) showed that, in response to increased rainfall in the Sahel, local SM feedbacks played a crucial role in low-level circulation changes and the positioning of the ITD.

Although the ITD and AEJ are both controlled by the regional temperature patterns and play important roles in the monsoon dynamics, investigations into their evolution and co-variance over the Sahel in wet and dry years have been limited. Nicholson and Grist (2001) developed a conceptual model to explain Sahelian rainfall variability during wet (1958–1967) and dry (1968–1997) periods. They observed that, in dry years, the AEJ tends to be positioned further southward, stronger, and associated with a more southerly ITD. Conversely, in wet years, they found the AEJ to be shifted northward, weaker, and aligned with a more northerly ITD (Newell & Kidson, 1984; Nicholson & Grist, 2001; Nicholson & Webster, 2007). The displacement of the AEJ during these phases is influenced by the strength of southwesterly low-level monsoon flow, which significantly affects shear instabilities (Nicholson, 2009). Furthermore, dry years are characterised by a contraction and weakening of the tropical rain belt compared with wet years, primarily due to meridional shifts in the AEJ (Nicholson, 2008). In other studies, the passage of mesoscale convective systems (MCSs) has been found to induce shifts in the AEJ's apparent latitudinal position, potentially causing the jet to bifurcate into a north and south position (Nicholson, 2013). Mohr and Thorncroft (2006) have highlighted that intense convective systems peak during the northward migration of the AEJ, distinct from weaker convective systems.

MCS organisation, structure, and maintenance is governed by the ingredients for deep moist convection (moisture, instability, and lift) and by how vertical wind shear interacts with convective updraughts and cold pools (Schumacher & Rasmussen, 2020). In southern West Africa, Maranan *et al.* (2018), using 16-year reflectivity data from the Tropical Rainfall Measuring Mission precipitation radar, found highly organised MCS events occurring in strongly sheared wind environments, whereas less organised convection occurred under a regime of low wind shear, deep westerly anomalies, and low to moderate convective available potential energy (CAPE). Over the same region, Nkrumah *et al.* (2023), using self-organising maps to classify various synoptic states driving MCSs in the West African monsoon, found that the synoptic states of most MCS days showed positive zonal wind shear (for 925 mb and 650 mb) anomalies that are linked to positive low-level temperature anomalies to the north of the region, further emphasising the role of warmer Sahelian surface

conditions in promoting favourable MCS conditions in southern West Africa. Baidu *et al.* (2022) also found strong vertical shear to be pivotal to long-lived, slow propagation, moderate sizes, and colder storms with high rain rates in western and Central Africa. Other studies support the role of AEJ shear on MCS evolution in West Africa (e.g., Bickle, 2021; Maybee *et al.*, 2024; Schrage *et al.*, 2006; Vizy & Cook, 2018) and elsewhere (e.g., Chen *et al.*, 2015; Cohen *et al.*, 2007; Taylor *et al.*, 2018).

Given the status of the Sahel as one of the most climate-sensitive regions globally (Nicholson, 2018), coupled with an observed rise in extreme rainfall events (Biasutti, 2019; Chagnaud *et al.*, 2022), understanding the dynamics of the ITD and AEJ, their variability, and the relationship to land-surface forcing is imperative. In fact, Taylor *et al.* (2017) found the identified trend in extreme Sahelian MCSs to be linked to changes in Saharan air layer and enhanced wind shear, which are strongly affected by ITD and AEJ positioning respectively. Though previous studies have characterised key features of Sahelian climate variability, this study uniquely integrates land–atmosphere interactions, surface energy budget dynamics, and SM anomalies with the spatio-temporal behaviour of the ITD, AEJ, and MCSs. This integrated approach provides a more holistic understanding of the mechanisms driving hydroclimatic variability in the Sahel. The study employs reanalysis data and observations to investigate the co-variability of the ITD and AEJ across the Sahel and implications of their positioning for MCS occurrence and intensity. Our analyses focus on the diurnal cycle of the ITD and AEJ, their relationship with surface fluxes, and the spatial distribution of warm and cold MCSs relative to these features.

2 | DATA AND METHODS

To select anomalous conditions of wet and dry years, we used rainfall of 41 years from the Climate Hazard and Infrared Precipitation with Stations (Funk *et al.*, 2015) data at a 0.25° × 0.25° longitude–latitude over the Sahelian region (latitudes 12°–20°N; longitudes 15°W–10°E). Ten wet years (1994, 1998, 1999, 2003, 2010, 2012, 2015, 2018, 2020, 2022) and 10 dry years (1982, 1983, 1984, 1987, 1990, 1991, 1993, 1996, 1997, 2002) were then selected based on the anomalies for further studies using a composite analysis approach. For each of these years, the corresponding surface products, such as SM, surface SH and LH, CAPE, and vertical profiles of geopotential height, specific and relative humidity (q and RH), vertical velocity and zonal wind (u and v) at pressure levels 925 mb to 400 mb, were obtained from the fifth-generation European Centre for Medium-Range Weather Forecasts Reanalysis (ERA5) at 0.25° × 0.25° longitude–latitude (Dee *et al.*, 2011). We tested the hypothesis that the AEJ is modulated by the meridional temperature gradient through SH, which is influenced by SM, by applying the boundary-layer heat budget expressed in Equation (1) by assuming a fixed planetary boundary-layer depth of 1 km.

$$\Delta T = \left(\frac{\Delta \mathrm{SH}}{\rho\, c_p \times \mathrm{pbl}} \right) \delta t, \tag{1}$$

where ΔT is the change in temperature over a time period, ΔSH is the change in accumulated heat via SH over a time period, ρ is the density of air (1.2 kg·m^{-3}), c_p is the specific heat capacity of dry air at constant pressure (1,004 J·kg^{-1} ·K^{-1}), and δt (s) is the change representing the time interval over which the energy flux is integrated.

The ITD is typically identified by the confluence of low-level winds, a strong gradient in moisture or temperature, or a surface dew-point temperature of approximately 14°C. Here, we used the 10 g · kg^{-1} specific humidity threshold as this study places particular emphasis on the spatial distribution of moisture, which plays a critical role in convection initiation and development. As indicated by Roberts *et al.* (2015), this threshold may correspond to slightly drier conditions than the 14°C dew-point criterion, but it remains a valuable indicator of the latitudinal extent of moisture advection by the monsoon flow. All the zonal averages shown are calculated between 15°W and 10°E to exclude any potential oceanic influence. Unless otherwise stated, the maximum easterly wind for the averaged vertical layer of 700–500 mb was used to identify the AEJ in this analysis. Finally, we conduct an MCS analysis for warm (−40°C) and cold (−70°C) cloud-top temperatures covering an area greater than 5000 km^2 as used in Klein *et al.* (2021), on data obtained from the Meteosat Second Generation satellite. Here, the −70°C MCSs constitute subgroups of the −40°C MCS sample, representing MCSs with wide convective cores that are more likely to produce very intense rainfall (see, Maranan *et al.*, 2018).

3 | RESULTS

In this study, we first give an overview of the rainfall pattern in anomalous wet and dry years. Then we show the variability of the ITD and AEJ, and their relationships to the regional thermodynamics, before demonstrating how surface forcing influences the system. Finally, we show the relative positioning of the features in relation to the cold and warm MCSs in the region.

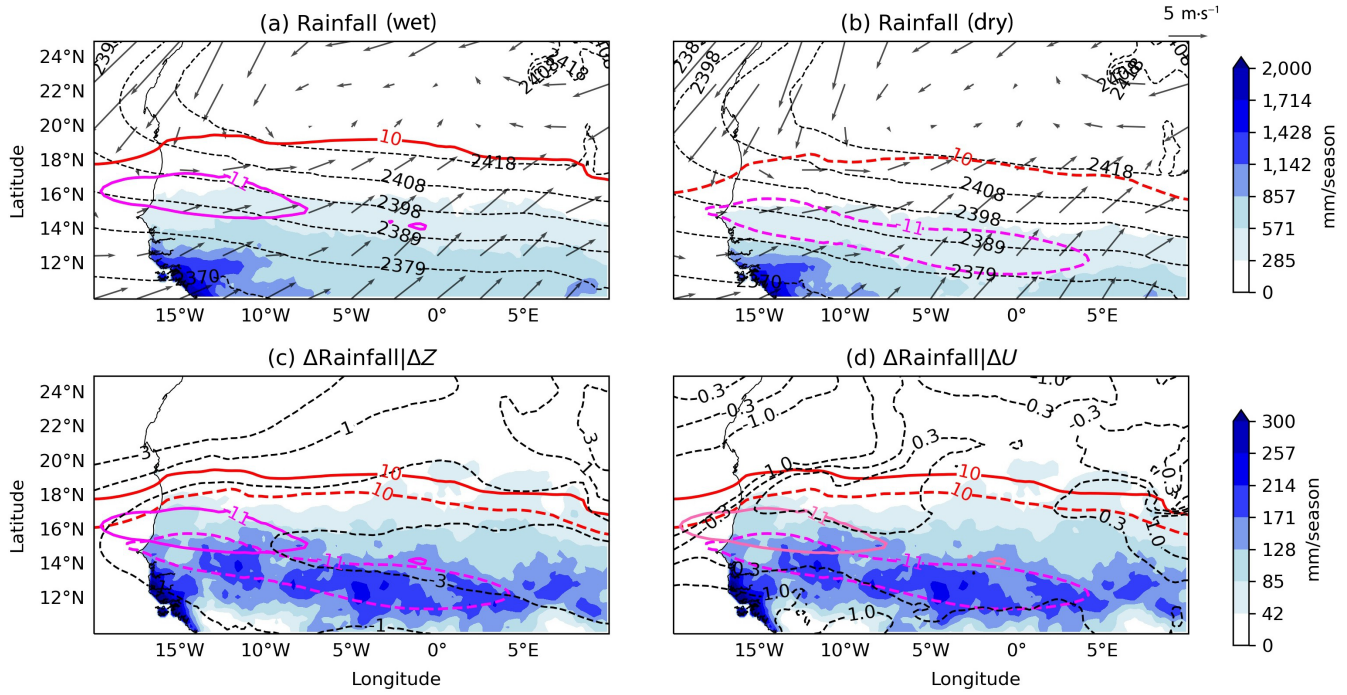

FIGURE 1 Spatial distributions in mean rainfall (mm/season) in July to September for (a) wet-year composites and (b) dry-year composites. Superimposed are the respective geopotential height Z difference between 700 mb and 925 mb (dashed black contours). The position of the African easterly jet (AEJ) core in wet and dry years is shown in solid and dashed pink respectively. The rainfall difference (shaded) is overlaid with geopotential height differences (wet minus dry; black dashed contours) and AEJ core contours in (c) and wind speed U contours (dashed black) in (d). The approximate mean location of the intertropical discontinuity (specific humidity of 10 g·kg^{-1}) is indicated with the solid and dashed red contours for wet and dry years respectively. Note that the Sahelian domain is between 15°W–10°E and 12–20°N. [Colour figure can be viewed at wileyonlinelibrary.com]

3.1 | Rainfall overview

Figure 1 shows a decade-long composite of wet- and dry-year rainfall anomalies averaged between July and September. These months fall within the active Sahelian monsoon season, which accumulates about 80% of the region's rainfall (Nicholson, 2008, 2013). The total seasonal rainfall of the wet- and dry-year composites shows a maximum in the western Sahel (Figure 1a,b) and a mean seasonal rainfall difference across the domain of 90 mm/season. Most of the differences between wet and dry years are evident in the intensity of the rainy season (Figure 1c,d; see Grist & Nicholson, 2001). The low-level circulation patterns are similar in both composites (Figure 1a,b). However, the wet years are forced by stronger low-level westerlies (Figure 1d) within shallower geopotential height (Figure 1c). The AEJ core and ITD are both displaced northward in the wet years and the AEJ core lies at the south of the Sahel in the dry years (Figure 1). The zonal maximum rainfall differences between wet and dry years occur within the AEJ core (Figure 1c,d), which indicates the role of the jet in rainfall processes over the Sahel.

3.2 | Diurnal cycle and covariance of the ITD and AEJ

To understand the covariance of ITD and AEJ, we first investigate their coupling dynamics during the wet and dry years, focusing on variations in the diurnal cycle. The ITD shows a strong diurnal cycle. It reaches its northernmost position at 0900 UTC, due to nocturnal advection of cool monsoonal southwesterlies (Parker & Diop-Kane, 2017). At 1800 UTC, the ITD retreats southward in response to daytime warming and associated turbulence in the boundary layer mixing out the thermal gradient (Kalapureddy *et al.*, 2010; Sultan *et al.*, 2007). The latitudinal location of the AEJ shows less diurnal variability compared with the ITD in both composites. Meanwhile, the diurnal meridional displacements in the ITD (Figure 2a) coincide with the intensification (weakening) of the jet core at 0900 UTC (1800 UTC) in both composites (Figure 2b).

Figure 2a also shows a strongly coupled ITD and AEJ, reaching their northernmost limits (≈ 2° further north) during the wet years compared with the dry years. Since the ITD and AEJ are closely related to the strength and meridional extent of moisture advection, and subsequently

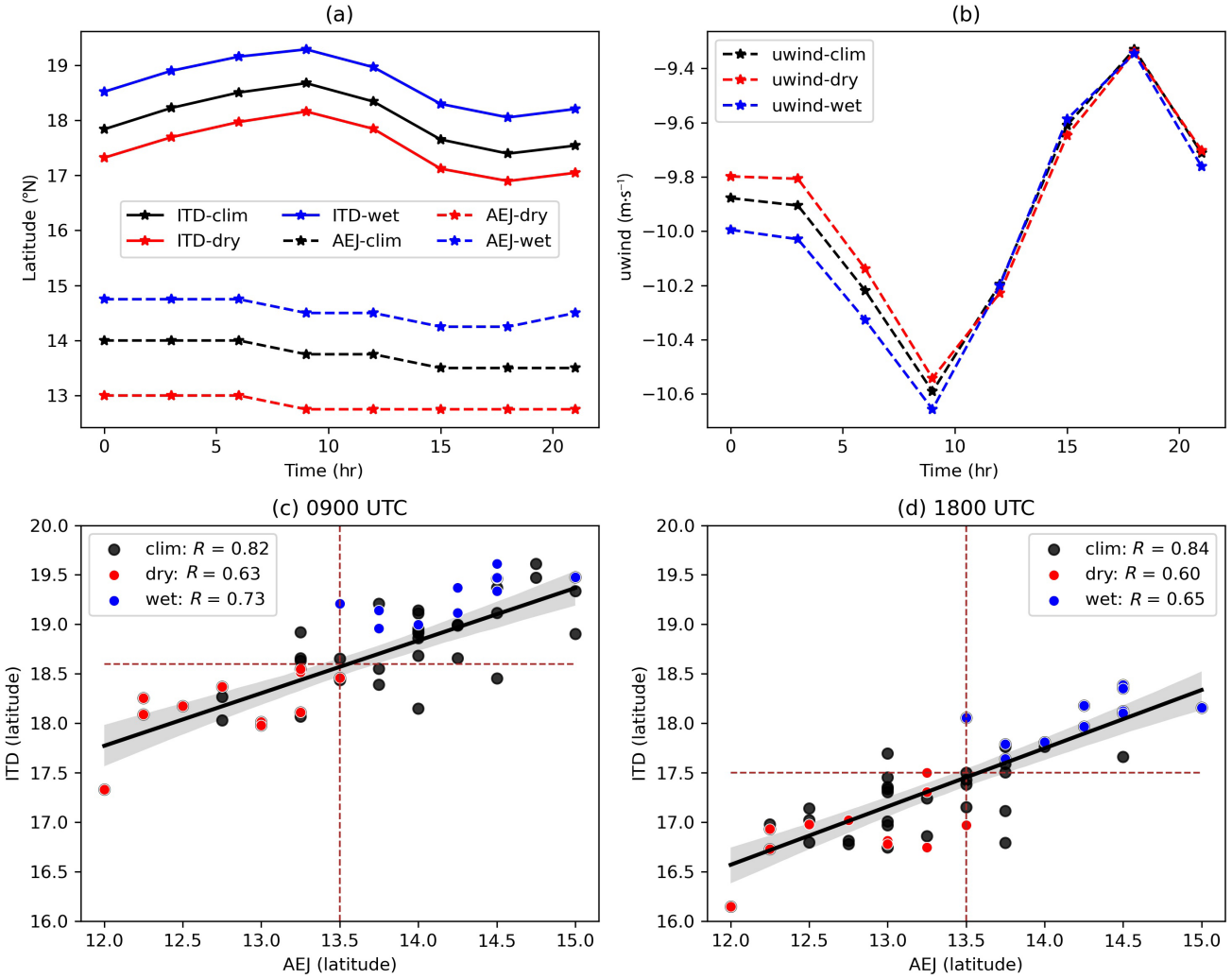

FIGURE 2 Zonally averaged (15°W to 10°E) diurnal (three-hourly) cycle for the climatology (clim) and wet and dry years, showing the (a) meridional variability of the intertropical discontinuity (ITD) and African easterly jet (AEJ), and (b) average of *u*-wind at 700–500 mb corresponding to the AEJ level. Regression of the ITD and AEJ at the times of (c) maximum (0900 UTC) and (d) minimum (1800 UTC) meridional limit using the Pearson correlation method. All coefficients are significant at $P \leq 0.05$. Dashed vertical lines separate the ITD–AEJ under wet and dry regimes. [Colour figure can be viewed at wileyonlinelibrary.com]

meridional gradients in temperature and moisture (Kalapureddy *et al.*, 2010), a constant distance between the two features could have been expected in both composites. Instead, from Figure 2a, the average distance between the ITD and AEJ is larger in dry years (5°) than in wet years (4°). This disparity is mainly controlled by their relative positioning over the eastern part of the Sahel, as observed in Figure 1. This behaviour could be linked to changes in convective activity and the sensitivity of the features to differences in the strength of the shallow meridional circulation in wet and dry years, as suggested by Zhang *et al.* (2008) and Shekhar and Boos (2017).

Dezfuli and Nicholson (2011) found that the intensity and location of the AEJ are uncorrelated in space and time, as also observed in Figure 2a,b. However, since both the jet and ITD positioning show a consistent displacement between wet and dry years (Figure 2a,b), we further examine their covariance by correlating them at the diurnal maximum (0900 UTC) and minimum (1800 UTC) for all individual years. Figure 2c,d reveals that in the majority of wet years the ITD (AEJ) is positioned north of 17.5°N (13.5°N) at time of maximum ITD southward excursion (1800 UTC), whereas dry years show more southward positioning. The ITD northward shift at night and the southward shift during the day are clearly visible in Figure 2c,d. This illustrates that wet (dry) years are characterised by a consistent northward (southward) shift of both ITD and AEJ, albeit with a smaller distance between them during wet years. The overall spread of the AEJ intensity, latitudinal positioning of the ITD and AEJ in wet, dry, and climatological years is shown in Supporting Information Figure S1.

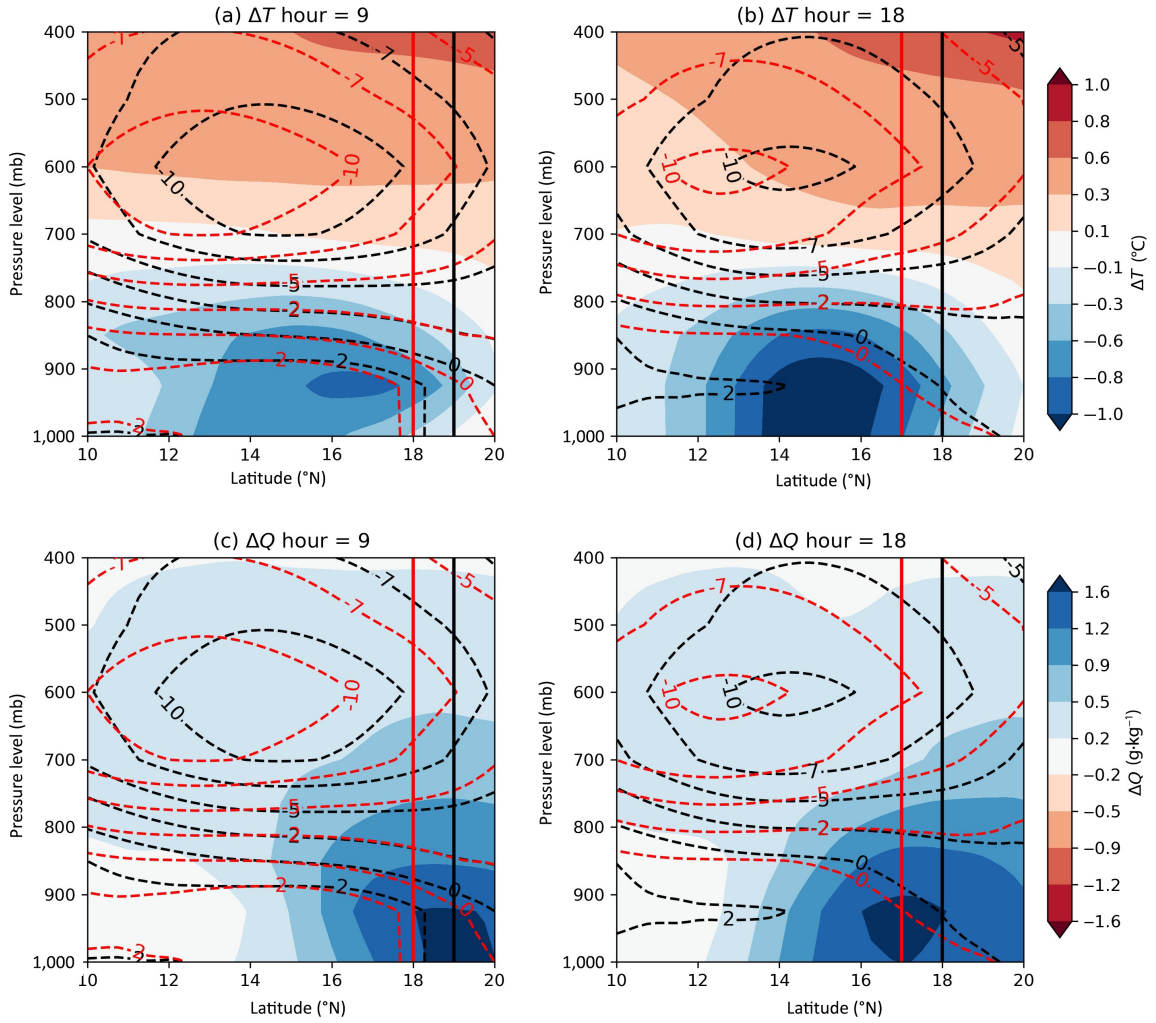

FIGURE 3 Zonally averaged vertical cross-section of the difference (wet minus dry) in temperature at (a) 0900 UTC and (b) 1800 UTC and (c, d) specific humidity at same times. Black and red contours are the zonal winds for wet and dry years respectively. The vertical solid vertical lines represent the location of the intertropical discontinuity for wet (black) and dry (years). The AEJ core denoted by the mid-tropsheric easterly contours of −10 m/s. For clarity, contours are spaced at 2 m·s^{-1} for westerlies and 3 m·s^{-1} for easterlies. [Colour figure can be viewed at wileyonlinelibrary.com]

3.3 | Vertical structure of temperature, moisture, and AEJ relative to the ITD

We now consider how the differences in low-level temperature and humidity affect the temperature gradient, geostrophic wind distribution and subsequently the ITD and AEJ positioning in both composites. Temperature differences modulate the overall temperature gradient, and the stability of the jet (Grist & Nicholson, 2001). These cross-sections were selected for hours of minimum and maximum ITD excursion and AEJ speed at 0900 UTC and 1800 UTC, as previously shown. From Figure 3a,b, wet years are characterised by a cool Sahelian boundary layer (12–18°N) in response to evaporative cooling from enhanced rainfall activity (Figure 1c,d). The differences are also markedly larger at 1800 UTC (Figure 3b) than at 0900 UTC (Figure 3a), consistent with weaker sensible heat and stronger latent heating due to increased SM. Warmer temperatures aloft possibly indicate increased latent heat release (Grist & Nicholson, 2001) and a warmer Saharan air layer to the north. The tropospheric profile is also more humid in the wet years than the dry years with enhanced mid-tropospheric moistening (Figure 3c,d) from convective activities.

Whereas Figure 2b illustrated the diurnal cycle of mean AEJ intensity, Figure 3 shows the spatial structure of the AEJ core (indicated by the −10 m·s^{-1} contours). There is no clear difference in jet core extent between the wet and dry years for either hour (Figure 3, black and red contours). However, its 0900 UTC vertical extent between 700 and 500 mb (Figure 3a,c) contracts to the 600 mb level by 1800 UTC (Figure 3b,d). The behaviour of the jet is similar to that reported by Nicholson and Grist (2001) and Nicholson (2009), who also observed a shift in the

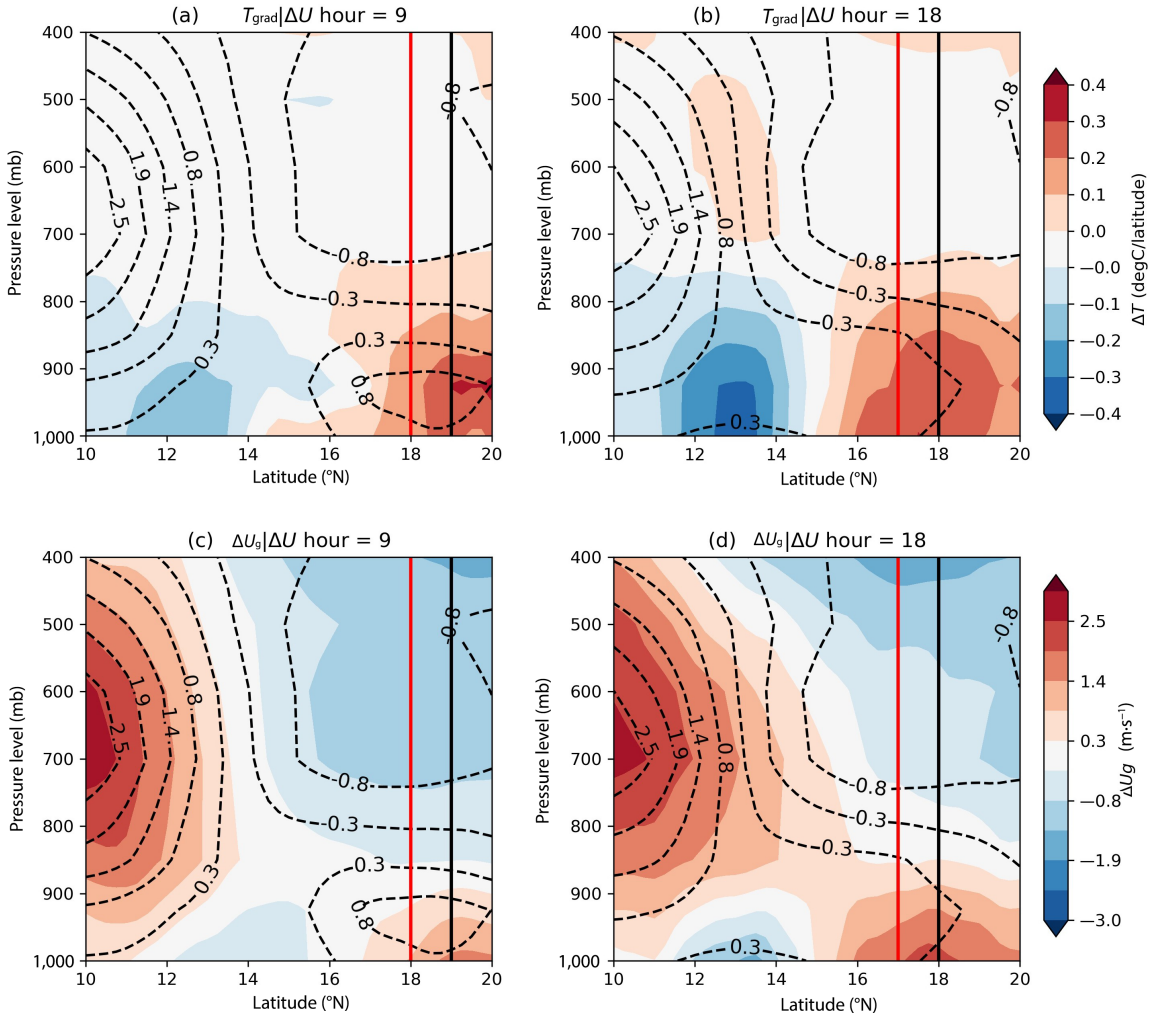

FIGURE 4 As Figure 3, but showing temperature gradient and zonal winds at (a) 0900 UTC and (b) 1800 UTC and (c, d) geostrophic wind at same times. The vertical solid vertical lines represent the location of the intertropical discontinuity for wet (black) and dry (years). [Colour figure can be viewed at wileyonlinelibrary.com]

location of the jet between wet and dry years. However, their studies focused on periods that were possibly much wetter, specifically wet years in the 1950s and 1960s and dry years from 1968 to 1997—which likely represent a wetter climatic regime than the years considered in the present analysis. Therefore, though the general pattern aligns, complete agreement is not necessarily expected due to differences in the periods examined. The structural disparity in the jet at 0900 UTC and 1800 UTC is likely a direct result of the redistribution of heat and momentum from convection, vertical mixing, and turbulence during the day in the Sahel, contributing to the upward shift and narrowing of the AEJ at 1800 UTC. The reverse occurs during the night in both composites, where reduced vertical mixing leads to a shallower and stabilised nocturnal boundary layer, which seems to help the jet "bulge" vertically at 0900 UTC, as the geostrophic winds weakens (Figure 4c).

For the ITD, its exact location is extremely sensitive to the strength of the monsoonal southwesterly flow in wet and dry years. At 0900 UTC for wet years, the impact of the monsoonal westerlies is strong and displaces the ITD about 0.5° north of the dry-year ITD (see Figure 3a,c). Meanwhile, at 1800 UTC the monsoonal flow is weak from daytime turbulent mixing and the ITD retreats south. This daytime retreat for the wet year is about 1° north of the dry year (see Figure 3b,d). The state of the land surface can also influence the location of the monsoon circulation, even when large-scale boundary conditions are held constant (Klein *et al.*, 2015; Mutton *et al.*, 2022; Talib *et al.*, 2022), and can induce a migration of the ITD by 1–2° latitude (Lothon *et al.*, 2008). For instance, the final daytime positioning of the ITD, although driven primarily by the nocturnal monsoon flux, may also be affected by local boundary-layer humidity dynamics through daytime evaporative processes. That is, excess surface moisture

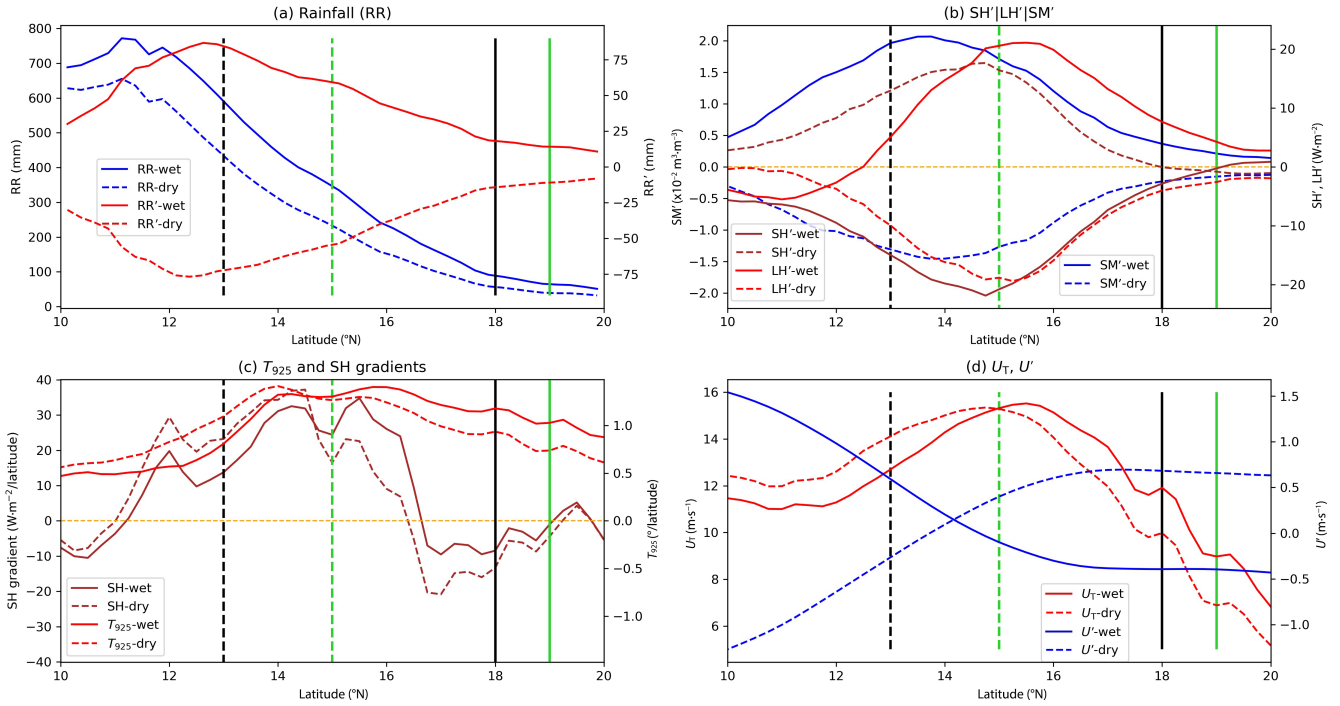

FIGURE 5 Zonal averages of (a) rainfall (RR) and its anomalies (RR′), (b) soil moisture (SM′), surface sensible and latent heat flux anomalies (SH′, LH′), (c) gradients in surface SH and low-level temperature (925 mb), and (d) thermal wind balance (difference between geostrophic wind at 925 mb and the average of 700–500 mb (U_T) and the mid-tropospheric zonal wind anomalies (U', 700–500 mb). All variables except the rainfall and soil moisture were sampled over 1200–1500 UTC. The mean locations of the intertropical discontinuity and African easterly jet in both composites are also indicated in dashed and solid black (dry years) and green (wet years) vertical lines, respectively. Finally, the meridional spread of these surface and wind variables is shown in Supporting Information Figure S2. [Colour figure can be viewed at wileyonlinelibrary.com]

increases low-level humidity, which is carried along by the monsoonal westerly flow and would subsequently affect the final location, where the humidity may drop below the 10 g·kg^{-1} ITD threshold. Conversely, enhanced warming over moisture-limited soils can lead to a deeper planetary boundary layer and thus mixing of humidity over a deeper layer, favouring a more southward ITD position. The presence of humidity anomalies a few degrees beyond the ITD has been reported by Parker *et al.* (2005) and Osei *et al.* (2023).

The surface-forced cooling in the wet years has direct implications on the temperature gradient, geostrophic wind and subsequently the structure of the AEJ. Studies have shown that the temperature gradient is essential for the formation and location of the AEJ (Cook, 1999; Nicholson & Grist, 2001; Pospichal & Crewell, 2007; Wu *et al.*, 2009). Figure 4a,b presents the differences in temperature gradient between wet and dry years, superimposed with the differences in zonal winds. In the wet years (Figure 4a,b), enhanced rainfall (see Figure 1c,d) and increased SM south of 15°N (Figure 5b) dampen land surface heating, shifting the temperature gradient northward, with the strongest difference at around 18°N. This is directly co-located with strengthened midlevel easterly winds, which are in geostrophic balance with the actual flow (Figure 4c,d), indicating the resulting AEJ shifts in the composites. The presence of enhanced atmospheric humidity through both monsoonal circulation and evapotranspiration in the wet years enhances baroclinicity across a more northern band than in dry years and thus explains the AEJ position over these locations in the wet years.

In addition, diurnally, the match of wind differences with geostrophic wind differences is quite close at 0900 UTC (Figure 4c) and at 1800 UTC to the south of 13°N (Figure 4d). However, at 1800 UTC to the north of 13°N, these differences are not so closely matched. In the afternoon, and still by 1800 UTC, the boundary layer in the north is dominated by a deep convective boundary layer that leads to intense vertical mixing and means that geostrophic balance can no longer dominate the dynamics. This is particularly clear at low levels at 1800 UTC, where the geostrophic wind difference is slightly stronger than its values at 0900 UTC, but the difference in actual winds is much weaker due to turbulent mixing and drag. Parker *et al.* (2005) found from dropsonde observations that the observed wind shear in the afternoon was only around 50% of the geostrophic wind shear for this reason.

Overall, these findings highlight the critical role of the temperature gradient in shaping the structure and behaviour of the geostrophic wind flow and subsequently the ITD and AEJ during wet and dry years. In addition, the gradient differences between both composites are crucial in detecting where the strongest regions that amplify the jet lie in both wet and dry years.

3.4 | Influence of surface fluxes on the ITD and AEJ

We now explore the conditions of surface processes that affect the stability of the AEJ and thermal wind balance. As previously stated, these processes have significant impact on boundary-layer dynamics, which ultimately affects the ITD and AEJ through vertical turbulent mixing. Since turbulent activities respond to changes in surface energy partitioning, we examine how the ITD and AEJ positioning in both composites align with SH and LH anomalies, all of which can be affected by SM differences. Soil moisture–circulation feedback in the Sahel also determines the low-level circulation changes and location of the ITD (Mutton *et al.*, 2022). We analyse these processes using two metrics: anomalies against climatology, which explain why these changes occur over specific parts of the domain, and gradients, which explain the shifts in jet locations.

Soil moisture changes depend largely on the variability, distribution, and intensity of rainfall. Similar to Figure 1, the maximum rainfall in Figure 5a sits in the southern Sahel but with maximum anomalous changes that lie about 1–2° south of the jet in the composites. The SM anomalies (Figure 5b) are concomitant with the rainfall anomalies (Figure 5a), resulting in shifts in the heat flux anomalies due to energy and moisture limitation regimes (Chen *et al.*, 2024; Feldman *et al.*, 2019) at the south and north of the Sahel respectively. Note that we do not expect observed rainfall differences between wet and dry years (Figure 5a) to exactly mirror top-layer SM differences in ERA5 (Figure 5b) as the latter is based on a combination of ERA5 rainfall, satellite SM, and screen-level temperature and humidity data and does not account for increases in runoff and infiltration under wetter conditions.

The AEJ is situated in the region of maximum SM sensitivity (14°–16°N), where the SH′ (negative) and LH′ (positive) are most pronounced (Figure 5b). This coincides with the zone where the SH gradients transition and reaches its maximum positive phase (Figure 5c). The temperatures increase via a stronger SH in the dry year, which is dampened by increased LH fluxes from SM evaporation in the wet year. In the dry composites, the AEJ location is mainly influenced by the SH flux and temperature gradients in a region that is less soil-moisture sensitive, located about 1° south (13°N) of the gradients' positive maxima (Figure 5c). The thermal wind strengthens around 16°N (north of the jet; Figure 5d), in balance with the largest positive SH and temperature gradients in both composites (compare Figure 5c and Figure 5d). The mid-tropospheric easterly wind anomalies (dashed lines; Figure 5d) confirm that wet years exhibit a northward displacement of the AEJ position, with stronger easterly winds north of 14°N relative to climatology. Dry years show the opposite pattern, with stronger easterly anomalies at all latitudes south of 14°N illustrating a southward displacement.

We further examine the hypothesis that the jet is linked to the meridional temperature gradient through SH, which in turn is modulated by SM using the heat budget equation. Across the Sahel, daytime SH (0900–1800 UTC) is consistently larger in dry years than in wet years, with the greatest enhancement near 13.5°N ($\sim 19\ \mathrm{W \cdot m^{-2}}$, Figure 6a). This additional flux in dry years corresponds to approximately $615{,}600\ \mathrm{J \cdot m^{-2}}$ over 9 hr, which would warm a 1-km-deep mixed layer by about 0.6°C (Figure 6b), consistent with the observed ERA5 difference of 0.5°C near 15°N (Figure 6c). Though our estimate assumes a fixed planetary boundary-layer depth with no mixing with the overlying air, and neglects advection, radiation, and evaporative cooling terms in the heat budget, the magnitude of SH contrast is sufficient to explain the primary strengthening of the meridional temperature gradient between wet and dry years. Small spatial offsets may arise because actual boundary-layer depth varies with latitude and other processes contribute to the heat budget.

In conclusion, rainfall differences have been shown to influence SM anomalies, which in turn modify SH anomalies and gradients throughout the Sahel. The temperature gradients respond to the SH modification and consistently appear just north of the AEJ for both wet and dry composites, contributing to adjustments in the thermal wind balance. The largest difference in these gradients is around 15°N, where they begin to diverge in the wet and dry years. This also marks the region where anomalies in SH and LH driven by soil moisture peak, and thus significantly affect both the energy partitioning and hence temperature gradients, which in turn influence the AEJ in these years.

3.5 | Distribution of MCSs relative to the ITD and AEJ

We now evaluate how MCS frequencies are affected by the displaced dynamical features of the WAM during wet and dry years. Looking at MCS seasonality over southern West Africa, Klein *et al.* (2021) identified a shear regime co-located and to the north of the AEJ that favours the

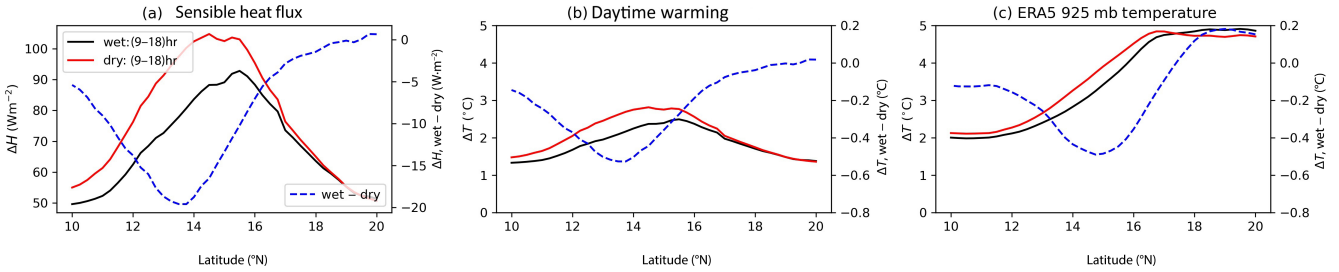

FIGURE 6 Meridional distribution of (a) daytime mean sensible heat flux, (b) contribution to daytime warming using Equation (1), and (c) total daytime warming in fifth-generation European Centre for Medium-Range Weather Forecasts Reanalysis (ERA5) temperature at 925 mb. Daytime refers to the period 0900 to 1800 UTC. The difference between wet (black) and dry (red) years is shown by the dashed blue line (secondary vertical axis). [Colour figure can be viewed at wileyonlinelibrary.com]

occurrence of particularly cold, intense MCSs compared with south of the AEJ, where near-moist adiabatic conditions and, hence, warmer MCSs prevail. Here, we conduct a similar examination for the Sahelian monsoon period, albeit on a wet and dry composite, considering the frequency distribution of warm (−40°C) and colder, more intense (−70°C) MCS subgroups relative to CAPE, the AEJ and its associated shear, and the ITD positioning. The AEJ affects MCS organisation and evolution by enhancing low-to-mid-level wind shear (Hodges & Thorncroft, 1997; Laing *et al.*, 2008; Mohr & Thorncroft, 2006), and the jet can also be perturbed by the passage of these storms (see Wang & Elsberry, 2010).

In all cases, warm MCSs are more frequent south of the main jet core, where the CAPE (Figure 7a–c) and vertical humidity gradient (Figure 7d–f) are both weak and the tropospheric profile shows deep moistening. Convection here is thus frequent due to the weak vertical humidity gradient, which acts to reduce convection inhibition considerably. Meanwhile, the cold MCSs (−70°C), which peak 2–3° north of the warm MCS peak, require a combination of low-level moisture and a strong shear regime to intensify (Figure 7d–f). These storms are closely aligned with the absolute jet core (thus where the AEJ is strongest) and CAPE is maximised by the low-level moisture tongue from the south, which is strongly capped by the mid-level dry air intrusion from the north and sensitive to land surface conditions (Figure 5b). Further comparison of the frequency anomaly of the cold storms with the CAPE and shear anomalies (Figure 8) reveals a distinct pattern of anomalous CAPE depletion by these storms below 14°N in the wet year. At the northern Sahel, both CAPE and shear become positive, enhancing storm frequency (Figure 8a), forced by anomalously high low-level humidity that enhances the storm frequency (Figure 8c). Concurrently, the anomalously low storm frequency at the north in dry years (Figure 8d) also shows a lower than normal CAPE in a drier than normal low-level tropospheric environment (Figure 8d).

The ITD plays a positive role on convection by producing strong convergence from daytime surface heating, especially over drier soils (Klein & Taylor, 2020), which generates turbulent mixing that promotes boundary-layer growth and is accompanied by a low-level reversal in the meridional flow (Vizy & Cook, 2018; Figure 7d–f). The active convection, in all composites, occurs about 2°–3° south of the ITD, where low-level moist conditions are present (Figure 7d–f) and vertical mixing extends to the level of free convection, favourable for storm formation. More stable conditions exist very close to the ITD in both composites (1°–2° south), leading to fewer well-organised storms possibly due to dry convection from dry conditions, weakly sheared environments (as in Mohr & Thorncroft, 2006), increased capping (dry mid-tropospere) with suppressed CAPE (Figure 7a–c), and the states of SM and surface heat fluxes (Figure 5b) found close to the ITD. The sharp northward decline in MCSs in the dry-year composite (Figure 7b) is further exacerbated by the drier low to mid-tropospheric moisture availability around the ITD due to a more southerly location of the monsoon. This dry troposphere around the ITD shows a humidity decline of about 3% below normal (Figure 8d). During wet years (Figure 7a), the moist low-level troposphere (4% above normal; Figure 8c) may occasionally break the cap, subsequently leading to a period of CAPE maximisation and intense shear (Figure 8a) and less dry air entrainment to actively support these northernmost localised storms. The climatology (Figure 7c,f) in all storm regimes also behaves similar to the wet and dry years (Figure 7a,b,d,e).

The shifts in these features in the wet, dry, and climatology composites show how they are intricately linked and with conditions transitioning from a deep moist environment south of the AEJ to a CAPE- and shear-dominated environment co-located with the AEJ core, affecting MCS convective intensities. The dynamics in all composites are similar in the Sahel, compared with the strong differences found earlier in the seasonal cycle over southern West Africa in Klein *et al.* (2021).

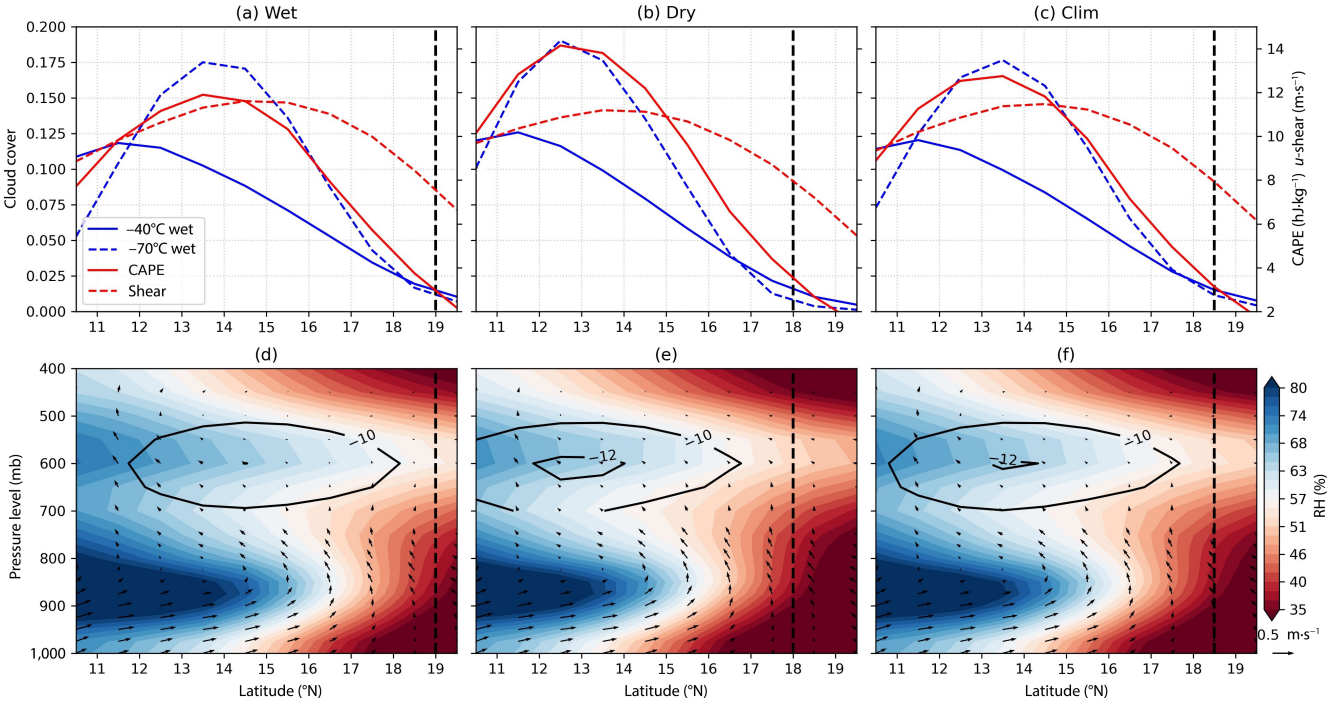

FIGURE 7 Line plots showing meridional frequency in cloud cover of both mesoscale convective system (MCS) types normalised by the total number of storm events for each composite, along with the convective available potential energy (CAPE; red solid lines) and African easterly jet (AEJ)-associated shear (u-shear between 925 and 500 mbar; red dashes), binned into 1° latitude as the MCSs for (a) wet, (b) dry and, (c) climatology (clim) years. (d)–(f) Cross-sections of relative humidity (RH, %; shading), zonal wind of the AEJ (black contours), and meridional circulation vectors (v wind, m·s^{-1}; $-\omega$, Pa·s^{-1}) for each corresponding composite with surface pressure masked to ensure accuracy. The vector scales in the vertical have been scaled to be faithful to the true angles of vectors in the coordinate system. The position of the intertropical discontinuity is denoted in the black vertical dashed lines. All zonal averages except for MCSs have been temporally sampled between 1200 and 1500 UTC and spatially between 15°W and 10°E. [Colour figure can be viewed at wileyonlinelibrary.com]

4 | DISCUSSIONS AND CONCLUSIONS

This study provides a comprehensive analysis of the covariance between the ITD and AEJ over the West African Sahel in wet and dry years. By leveraging a decade of observational and reanalysis data for each composite, we examined their diurnal variability, the thermodynamic and surface flux dynamics governing their formation, and their spatial relationship with MCSs for the July to September season.

Our findings highlight a strong coupling between the ITD and AEJ during wet years due to an intensified monsoonal flow. The AEJ position is relatively stable, showing weak diurnal variation in its location for both wet and dry years, whereas the AEJ intensity and ITD show strong diurnal cycles. The distance between the latitudinal positions of the ITD and AEJ is smaller in the wet years than in the dry years, which is likely driven by increased convective activity and sensitivity of the features to the shallow meridional circulation (Shekhar & Boos, 2017; Zhang *et al.*, 2008). The largest difference in jet intensities between wet and dry years occurs overnight (0000–0300 UTC) as opposed to daytime (1200–2100 UTC; Figure 2b). From 1200 UTC to 2100 UTC, the lower troposphere, up to the level of the AEJ, is more strongly influenced by dry convection in the north and shallow and congestus convection to the south (Parker *et al.*, 2005). These effects dampen the low-level monsoon meridional circulation and therefore may act to reduce these differences between the wet and dry years. At night, the low-level flow responds more freely to the low-level temperature contrasts and the circulation may be seen to respond more strongly to differences between wet and dry years, with the northerly return flow around jet level acting to enhance the AEJ through the Coriolis effect. In addition, tropospheric preconditioning, such as enhanced active nocturnal convection forced by deep equatorial westerlies, can cool the lower troposphere, leading to geostrophic wind adjustments in a stable boundary layer that can also act to intensify the jet overnight in wet years (Grist & Nicholson, 2001). The dynamics of the Saharan mineral dust may also influence these observations, as Bercos-Hickey *et al.* (2020) found a stronger AEJ in wetter and dusty years than in drier and less dusty years, although it is unclear the time of day for which these observations hold. The slopes of the ITD–AEJ

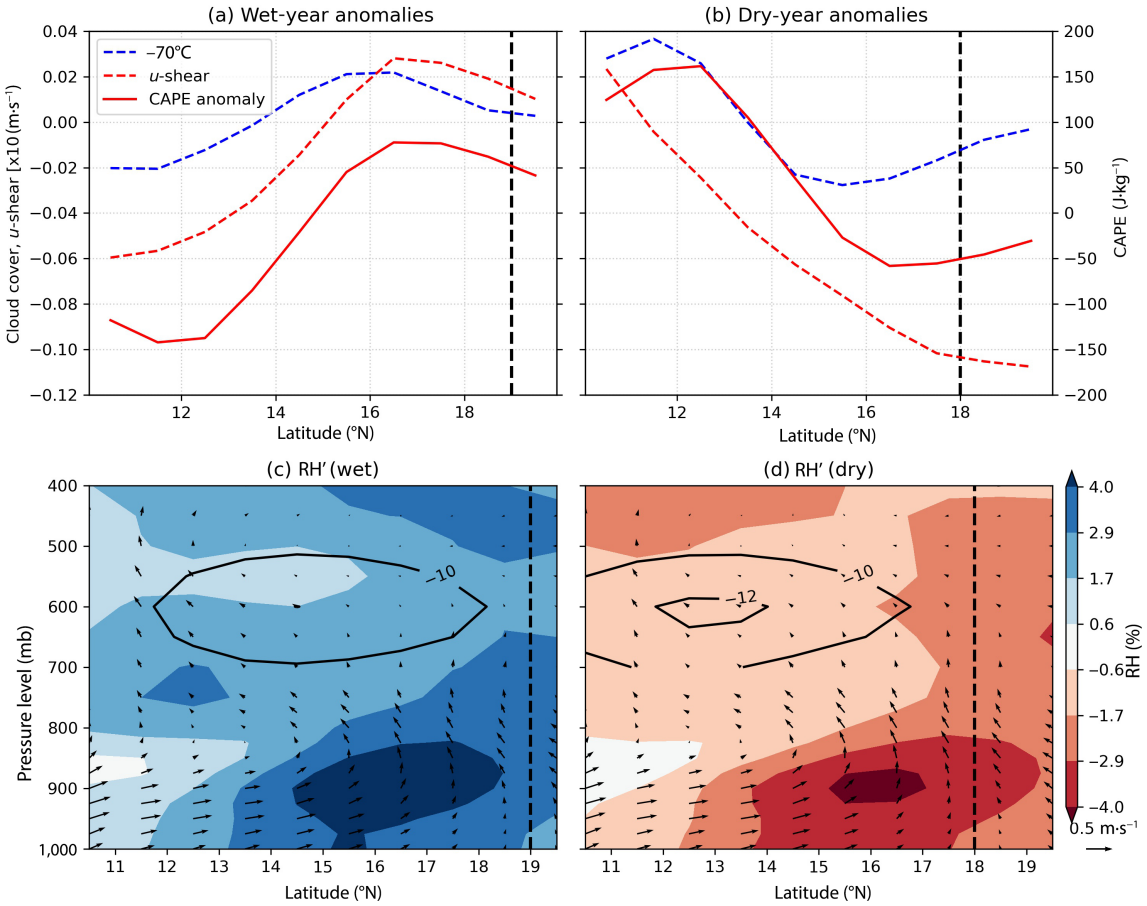

FIGURE 8 Meridional anomalies in −70°C mesoscale convective system, convective available potential energy (CAPE), and shear for (a) wet and (b) dry years. (c, d) Anomalies in the surface to mid-tropospheric relative humidity (RH) in the (c) wet and (d) dry years. The lines of wind vectors, intertropical discontinuity, and African easterly jet are same as in Figure 7. [Colour figure can be viewed at wileyonlinelibrary.com]

covariance are similar at 0900 UTC and 1800 UTC in both years, suggesting that though the ITD–AEJ distance exhibits diurnal variability due to the ITD's movement, the interannual displacement remains consistent throughout the day. A strong Saharan heat low intensifies the AEJ and tends to strengthen the southwesterly monsoon and the northeasterly Harmattan flow (Lavaysse *et al.*, 2010a, 2010b), thus modulating the co-variance of the jet and ITD.

Considering land-surface effects, differences in the SM driven by rainfall anomalies are not exactly co-located with heat flux anomalies, but strongly modulate the flux gradients. This anomaly discrepancy arises from the energy and moisture limitations (Chen *et al.*, 2024; Feldman *et al.*, 2019) in the southern and northern Sahel respectively. The SM anomalies influence AEJ positioning through SH anomalies most markedly at 15°N, which consistently shifts the jet south of SH and temperature gradient peaks. The thermal wind correlates better with lower tropospheric meridional temperature gradients particularly at 850 mb (see Parker & Diop-Kane, 2017). But at 925 mb the anomalies in sensible and latent heating shift the maximum thermal wind in the wet and dry years similarly to the north of the respective AEJ positions. Meanwhile, in all cases, the ITD is located at the tail of the gradient and anomaly distribution in the surface processes, suggesting less of an impact of soil-moisture-modulated surface fluxes on its location.

The spatial distribution of MCSs in wet and dry years is similar, with exceptions that storms occur more frequently in wet years and cold storms exhibit a more pronounced northward shift, whereas warm storms remain in the same location regardless of the year. Warm cloud systems preferentially form south of the AEJ in a moist, weakly sheared environment, where the vertical humidity gradient is also weak. On interannual time-scales, the colder, deeper storms align with the jet core, where strong low-level moisture, mid-tropospheric dryness, and significant shear and CAPE enhance storm organisation and intensity, with similar findings on the intraseasonal time-scale by Talib *et al.* (2022). The stronger shear conditions ensure that these cold storms are long-lived and have moderate speed and size with high rain rates (Baidu *et al.*, 2022) through

the separation of updraughts, downdraughts, and reduced dry air entrainment (Houze Jr, 2004; Schumacher & Rasmussen, 2020). Mohr and Thorncroft (2006) also found that these thermodynamic ingredients occurring in the vicinity of high terrain appeared to have the greatest probability of generating intense convective systems. The cold storms in all composites are also maximised about 600 km south of the ITD. About 200 km to the south of the ITD, in the so-called weather zone B (Fink *et al.*, 2017; Hamilton *et al.*, 1945), only a few MCSs occur; those that are able to overcome the strong mid-tropospheric capping initiate and can be well-organised and intense, but they remain short-lived (Fink *et al.*, 2017).

The ITD is known to have a positive impact on MCSs by promoting convergence and vertical mixing close to its vicinity (Klein & Taylor, 2020; Vizy & Cook, 2018). However, it does not appear to have a strong link to anomalous changes in SH and LH via SM in the time-scale considered in this study, but it may respond to shorter time-scales, particularly when sampled in late afternoon under localised thermodynamic modifications (e.g., Klein & Taylor, 2020). Overall, this study underscores the intricate interplay between the ITD, AEJ, and regional convective activity, providing critical insights into their co-variability in different rainfall regimes. Given the increasing variability in Sahelian precipitation patterns, these findings contribute to improving storm predictability and advancing our understanding of atmospheric dynamics in a changing climate.

ACKNOWLEDGEMENTS

Marian Amoakowaah Osei was funded by the Royal Society's Newton International Fellowship (NIF\R1\211183). Cornelia Klein acknowledges funding from the Natural Environment Research Council (NERC) under the independent research fellowship for the COCOON project (NE/X017419/1). We also thank the ERA5 and Climate Hazard and Infrared Precipitation with Stations teams for making their datasets freely available at https://cds.climate.copernicus.eu/datasets and https://data.chc.ucsb.edu/products/CHIRPS-2.0/global_daily/netcdf/p25/ respectively. Finally, we sincerely thank Professor Sharon Nicholson and the anonymous reviewer for their careful review of the manuscript and for their valuable suggestions and advice that have greatly improved the quality of this work.

CONFLICT OF INTEREST

The authors declare no conflicts of interest.

DATA AVAILABILITY STATEMENT

The data that support the findings of this study are openly available in the ECMWF Climate Data Store at https://cds.climate.copernicus.eu/datasets/reanalysis-era5-single-levels-monthly-means?tab=download, reference number 10.24381/cds.f17050d7.

ORCID

Christopher M. Taylor https://orcid.org/0000-0002-0120-3198
Douglas J. Parker https://orcid.org/0000-0003-2335-8198

REFERENCES

Baidu, M., Schwendike, J., Marsham, J.H. & Bain, C. (2022) Effects of vertical wind shear on intensities of mesoscale convective systems over West and Central Africa. *Atmospheric Science Letters*, 23, e1094.

Bercos-Hickey, E., Nathan, T.R. & Chen, S.-H. (2020) On the relationship between the African Easterly Jet, Saharan mineral dust aerosols, and West African precipitation. *Journal of Climate*, 33, 3533–3546.

Biasutti, M. (2019) Rainfall trends in the African Sahel: characteristics, processes, and causes. *Wiley Interdisciplinary Reviews: Climate Change*, 10, e591.

Bickle, M.E. (2021) *The role of wind shear in organised deep moist convection in the West African Monsoon*. (Ph.D. thesis, University of Leeds).

Chagnaud, G., Panthou, G., Vischel, T. & Lebel, T. (2022) A synthetic view of rainfall intensification in the West African Sahel. *Environmental Research Letters*, 17, 044005.

Chen, Q., Fan, J., Hagos, S., Gustafson Jr W. I. & Berg, L. K. (2015) Roles of wind shear at different vertical levels: cloud system organization and properties. *Journal of Geophysical Research: Atmospheres*, 120, 6551–6574.

Chen, X., Pan, Z., Huang, B., Liang, J., Wang, J., Zhang, Z. et al. (2024) Influence paradigms of soil moisture on land surface energy partitioning under different climatic conditions. *Science of the Total Environment*, 916, 170098.

Cohen, A.E., Coniglio, M.C., Corfidi, S.F. & Corfidi, S.J. (2007) Discrimination of mesoscale convective system environments using sounding observations. *Weather and Forecasting*, 22, 1045–1062.

Cook, K.H. (1999) Generation of the African Easterly Jet and its role in determining West African precipitation. *Journal of Climate*, 12, 1165–1184.

Cornforth, R., Mumba, Z., Parker, D.J., Berry, G., Chapelon, N., Diakaria, K. et al. (2017) *Synoptic systems. Meteorology of Tropical West Africa: the forecasters' handbook*. USA: Wiley Online Library. pp. 40–89.

Dee, D.P., Uppala, S.M., Simmons, A.J., Berrisford, P., Poli, P., Kobayashi, S. et al. (2011) The ERA-Interim reanalysis: configuration and performance of the data assimilation system. *Quarterly Journal of the Royal Meteorological Society*, 137, 553–597.

Dezfuli, A.K. & Nicholson, S.E. (2011) A note on long-term variations of the African easterly jet. *International Journal of Climatology*, 31, 2049–2054.

Feldman, A.F., Short Gianotti, D.J., Trigo, I.F., Salvucci, G.D. & Entekhabi, D. (2019) Satellite-based assessment of land surface energy partitioning–soil moisture relationships and

effects of confounding variables. *Water Resources Research*, 55, 10657–10677.

Fink, A. H., Engel, T., Ermert, V., Van Der Linden, R., Schneidewind, M., Redl, R., Afiesimama, E., Thiaw, W. M., Yorke, C., Evans, M. et al (2017) *Mean climate and seasonal cycle*, Placeholder Text1–39. USA: Wiley Online Library.

Funk, C., Peterson, P., Landsfeld, M., Pedreros, D., Verdin, J., Shukla, S. et al. (2015) The Climate Hazards Infrared Precipitation with Stations-a new environmental record for monitoring extremes. *Scientific Data*, 2, 1–21.

Grist, J.P. & Nicholson, S.E. (2001) A study of the dynamic factors influencing the rainfall variability in the West African Sahel. *Journal of Climate*, 14, 1337–1359.

Hamilton, R., Archbold, J. & Douglas, C. (1945) Meteorology of Nigeria and adjacent territory. *Quarterly Journal of the Royal Meteorological Society*, 71, 231–264.

Hodges, K.I. & Thorncroft, C. (1997) Distribution and statistics of African mesoscale convective weather systems based on the ISCCP Meteosat imagery. *Monthly Weather Review*, 125, 2821–2837.

Houze, R.A., Jr. (2004) Mesoscale convective systems. *Reviews of Geophysics*, 42, 1–43.

Kalapureddy, M., Lothon, M., Campistron, B., Lohou, F. & Saïd, F. (2010) Wind profiler analysis of the African Easterly Jet in relation with the boundary layer and the Saharan heat-low. *Quarterly Journal of the Royal Meteorological Society*, 136, 77–91.

Klein, C. & Taylor, C.M. (2020) Dry soils can intensify mesoscale convective systems. *Proceedings of the National Academy of Sciences*, 117, 21132–21137.

Klein, C., Heinzeller, D., Bliefernicht, J. & Kunstmann, H. (2015) Variability of West African monsoon patterns generated by a WRF multi-physics ensemble. *Climate Dynamics*, 45, 2733–2755.

Klein, C., Nkrumah, F., Taylor, C.M. & Adefisan, E.A. (2021) Seasonality and trends of drivers of mesoscale convective systems in southern West Africa. *Journal of Climate*, 34, 71–87.

Laing, A.G., Carbone, R., Levizzani, V. & Tuttle, J. (2008) The propagation and diurnal cycles of deep convection in northern tropical Africa. *Quarterly Journal of the Royal Meteorological Society*, 134, 93–109.

Lavaysse, C., Flamant, C. & Janicot, S. (2010a) Regional-scale convection patterns during strong and weak phases of the Saharan heat low. *Atmospheric Science Letters*, 11, 255–264.

Lavaysse, C., Flamant, C., Janicot, S. & Knippertz, P. (2010b) Links between African easterly waves, midlatitude circulation and intraseasonal pulsations of the West African heat low. *Quarterly Journal of the Royal Meteorological Society*, 136, 141–158.

Lothon, M., Saïd, F., Lohou, F. & Campistron, B. (2008) Observation of the diurnal cycle in the low troposphere of West Africa. *Monthly Weather Review*, 136, 3477–3500.

Maranan, M., Fink, A.H. & Knippertz, P. (2018) Rainfall types over southern West Africa: objective identification, climatology and synoptic environment. *Quarterly Journal of the Royal Meteorological Society*, 144, 1628–1648.

Maybee, B., Marsham, J.H., Klein, C.M., Parker, D.J., Barton, E.J., Taylor, C.M. et al. (2024) Wind shear effects in convection–permitting models influence MCS rainfall and forcing of tropical circulation. *Geophysical Research Letters*, 51, e2024GL110119.

Mohr, K.I. & Thorncroft, C.D. (2006) Intense convective systems in West Africa and their relationship to the African Easterly Jet. *Quarterly Journal of the Royal Meteorological Society: A Journal of the Atmospheric Sciences, Applied Meteorology and Physical Oceanography*, 132, 163–176.

Mutton, H., Chadwick, R., Collins, M., Lambert, F.H., Geen, R., Todd, A. et al. (2022) The impact of the direct radiative effect of increased CO2 on the West African Monsoon. *Journal of Climate*, 35, 2441–2458.

Newell, R.E. & Kidson, J.W. (1984) African mean wind changes between Sahelian wet and dry periods. *Journal of Climatology*, 4, 27–33.

Nicholson, S.E. (2008) The intensity, location and structure of the tropical rainbelt over west Africa as factors in interannual variability. *International Journal of Climatology: A Journal of the Royal Meteorological Society*, 28, 1775–1785.

Nicholson, S.E. (2009) On the factors modulating the intensity of the tropical rainbelt over West Africa. *International Journal of Climatology: A Journal of the Royal Meteorological Society*, 29, 673–689.

Nicholson, S.E. (2013) The West African Sahel: a review of recent studies on the rainfall regime and its interannual variability. *ISRN Meteorology*, 2013, 453521.

Nicholson, S.E. (2018) The ITCZ and the seasonal cycle over equatorial Africa. *Bulletin of the American Meteorological Society*, 99, 337–348.

Nicholson, S.E. & Grist, J. (2001) A conceptual model for understanding rainfall variability in the West African Sahel on interannual and interdecadal timescales. *International Journal of Climatology*, 21, 1733–1757.

Nicholson, S.E. & Webster, P.J. (2007) A physical basis for the interannual variability of rainfall in the Sahel. *Quarterly Journal of the Royal Meteorological Society*, 133, 2065–2084.

Nkrumah, F., Klein, C., Quagraine, K.A., Berkoh-Oforiwaa, R., Klutse, N.A.B., Essien, P. et al. (2023) Classification of large-scale environments that drive the formation of mesoscale convective systems over southern West Africa. *Weather and Climate Dynamics*, 4, 773–788.

Osei, M.A., Ferguson, C.R., Quansah, E., Padi, M., Amekudzi, L.K. & Danuor, S. (2023) West Africa's moist convective environment as observed by the Atmospheric InfraRed Sounder (AIRS). *International Journal of Climatology*, 43, 2428–2448.

Parker, D.J. & Diop-Kane, M. (2017) *Meteorology of tropical West Africa: the forecasters handbook*. USA: John Wiley & Sons.

Parker, D.J., Thorncroft, C.D., Burton, R.R. & Diongue-Niang, A. (2005) Analysis of the African easterly jet, using aircraft observations from the JET2000 experiment. *Quarterly Journal of the Royal Meteorological Society*, 131, 1461–1482.

Pospichal, B. & Crewell, S. (2007) Boundary layer observations in West Africa using a novel microwave radiometer. *Meteorologische Zeitschrift*, 16, 513–524.

Roberts, A.J., Marsham, J.H. & Knippertz, P. (2015) Disagreements in low-level moisture between (re) analyses over summertime West Africa. *Monthly Weather Review*, 143, 1193–1211.

Schrage, J.M., Fink, A.H., Ermert, V. & Ahlonsou, E.D. (2006) Three MCS cases occurring in different synoptic environments in the sub-Sahelian wet zone during the 2002 West African monsoon. *Journal of the Atmospheric Sciences*, 63, 2369–2382.

Schumacher, R.S. & Rasmussen, K.L. (2020) The formation, character and changing nature of mesoscale convective systems. *Nature Reviews Earth & Environment*, 1, 300–314.

Shekhar, R. & Boos, W.R. (2017) Weakening and shifting of the Saharan shallow meridional circulation during wet years of the West African monsoon. *Journal of Climate*, 30, 7399–7422.

Sultan, B. & Janicot, S. (2003) The West African monsoon dynamics. Part II: the preonset and onset of the summer monsoon. *Journal of Climate*, 16, 3407–3427.

Sultan, B., Janicot, S. & Drobinski, P. (2007) Characterization of the diurnal cycle of the West African monsoon around the monsoon onset. *Journal of Climate*, 20, 4014–4032.

Talib, J., Taylor, C.M., Klein, C., Harris, B.L., Anderson, S.R. & Semeena, V.S. (2022) The sensitivity of the West African monsoon circulation to intraseasonal soil moisture feedbacks. *Quarterly Journal of the Royal Meteorological Society*, 148, 1709–1730.

Taylor, C.M., Belušić, D., Guichard, F., Parker, D.J., Vischel, T., Bock, O. et al. (2017) Frequency of extreme Sahelian storms tripled since 1982 in satellite observations. *Nature*, 544, 475–478.

Taylor, C.M., Fink, A.H., Klein, C., Parker, D.J., Guichard, F., Harris, P.P. et al. (2018) Earlier seasonal onset of intense mesoscale convective systems in the Congo Basin since 1999. *Geophysical Research Letters*, 45, 13–458.

Thorncroft, C. & Blackburn, M. (1999) Maintenance of the African easterly jet. *Quarterly Journal of the Royal Meteorological Society*, 125, 763–786.

Tompkins, A., Diongue-Niang, A., Parker, D. & Thorncroft, C. (2005) The African easterly jet in the ECMWF integrated forecast \d Nsystem: 4D-Var analysis. *Quarterly Journal of the Royal Meteorological Society: A Journal of the Atmospheric Sciences, Applied Meteorology and Physical Oceanography*, 131, 2861–2885.

Vizy, E.K. & Cook, K.H. (2018) Mesoscale convective systems and nocturnal rainfall over the West African Sahel: role of the Inter-tropical front. *Climate Dynamics*, 50, 587–614.

Wang, Z. & Elsberry, R.L. (2010) Modulation of the African easterly jet by a mesoscale convective system. *Atmospheric Science Letters*, 11, 169–174.

Wu, M.-L.C., Reale, O., Schubert, S.D., Suarez, M.J., Koster, R.D. & Pegion, P.J. (2009) African easterly jet: structure and maintenance. *Journal of Climate*, 22, 4459–4480.

Zhang, C., Nolan, D.S., Thorncroft, C.D. & Nguyen, H. (2008) Shallow meridional circulations in the tropical atmosphere. *Journal of Climate*, 21, 3453–3470.

SUPPORTING INFORMATION

Additional supporting information can be found online in the Supporting Information section at the end of this article.

How to cite this article: Amoakowaah Osei, M., Klein, C., Taylor, C.M., Parker, D.J. & Baidu, M. (2026) Covariance of the intertropical discontinuity and African easterly jet in Sahelian wet and dry years. *Quarterly Journal of the Royal Meteorological Society*, e70123. Available from: https://doi.org/10.1002/qj.70123